Autonomous Battery Equalization Module Using Capacitively Coupled Input-Parallel Output-Series Structure

Zhengqi Wei, *Graduate Student Member, IEEE*, Henry Shu-Hung Chung, *Fellow, IEEE*, and Ruihong Zhang, *Member, IEEE*

***Abstract*—An autonomous battery equalization module, which utilizes an energy circulation technique to equalize the voltage across individual battery cells in a series-connected batteries, is presented. Its structure consists of two power conversion stages. The first stage converts the battery string voltage into a high-frequency ac voltage to form a capacitively coupled ac link. The second one contains multiple diode-based rectifiers with their inputs connected to the ac link via coupling capacitors and their outputs connected in series to individual battery cells. Based on the property that the coupling capacitor voltage equals the battery cell voltage, and the rectifier input voltage are shared across the ac link, the magnitude of the current delivered by the second-stage converter is determined by the difference between the coupling capacitor voltage and the ac-link voltage. As the current taken from the first stage is common to all battery cells, charging or discharging of individual battery cells is autonomously adjusted by the output current of the second stage. Apart from equalizing the voltage of the battery cells within a module, the proposed architecture also allows multiple modules connected via the ac link. Individual battery cell can be charged by or discharged to the rest of battery cells in the same module or other modules. Two four-cell modules for equalizing eight 3.6 V, 18 650 batteries have been built and evaluated.**

***Index Terms*—Battery equalizer, battery management system, cell balancing, energy storage systems (ESSs), lithium-ion batteries.**

I. Introduction

LITHIUM-ION batteries have gained significant interest as viable solutions for large-scale energy storage systems (ESSs) and electric vehicles (EVs) owing to their high energy density and no memory effect [1], [2]. The market is currently populated with a considerable number of EVs, and the market has witnessed a rapid expansion, with sales soaring at an impressive pace [3], [4]. However, with the growing prevalence of the EVs, it is foreseeable that the global community will face a substantial quantity of retired EVs batteries in the future. Since these retired batteries are still usable, they can be used to construct ESS, suitable for stationary applications [5]. As shown in Fig. 1, battery-based ESS technology can realize bidirectional energy transfer with the power grid, making use of clean energy, sourced from collocated solar or wind plants [6], [7], [8]. While lithium-ion batteries are typically connected in series and are operated with the same current, their performance conformity tends to decline over long-term usage, leading to variations in their electrochemical characteristics [9]. This deterioration leads to diminished capacity within the battery pack, potentially causing overcharging and overdischarging of individual battery cells. Ultimately, this compromises the overall lifespan of the battery. A battery equalizer is thus of utmost importance in preserving the overall state of health (SOH) and durability of a series-connected battery pack. Its primary function is to equalize the state of charge (SOC) of each battery cell, thus avoiding possible overcharging or -discharging [10].

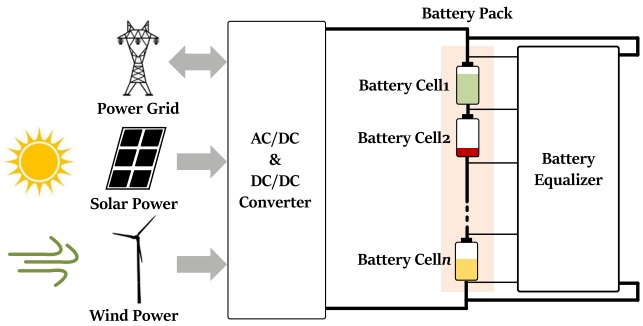

Fig. 1. Typical structure of battery-based ESSs.

Battery equalization structures can be categorized into four main types [11] as follows. Cell-to-cell (C2C) [12], energy buffer-based cell-to-cell (EBC2C) [13], [14], direct cell-to-cell (DC2C) [15], [16], [17], hierarchical module equalizer (HME) [18], [19], and stack-to-cell (S2C) [20], [21], [22], [23], [24], [25], [26]. They are shown in Fig. 2. In Fig. 2(a), a dc/dc converter is connected in every two batteries. The structure has several advantages, including simple structure, low cost, small volume, low voltage stress, and easy implementation. However, when battery mismatch occurs, the battery with a higher SOC

Received 7 September 2024; revised 10 November 2024; accepted 9 December 2024. Date of publication 16 December 2024; date of current version 28 January 2025. This work was supported by the Green Tech Fund from the Hong Kong Special Administrative Region, China, under Grant GTF202020166. Recommended for publication by Associate Editor K. Basu. *(Corresponding author: Henry Shu-Hung Chung.)*

Zhengqi Wei and Henry Shu-Hung Chung are with the Centre for Smart Energy Conversion and Utilization Research, Department of Electrical Engineering, City University of Hong Kong, Hong Kong (e-mail: zqwei5-c@my.cityu.edu.hk; eeshc@cityu.edu.hk).

Ruihong Zhang is with BYD Auto Industry Company Ltd., Shenzhen 518118, China (e-mail: zhang.ruihong2@byd.com).

Color versions of one or more figures in this article are available at https://doi.org/10.1109/TPEL.2024.3518552.

Digital Object Identifier 10.1109/TPEL.2024.3518552

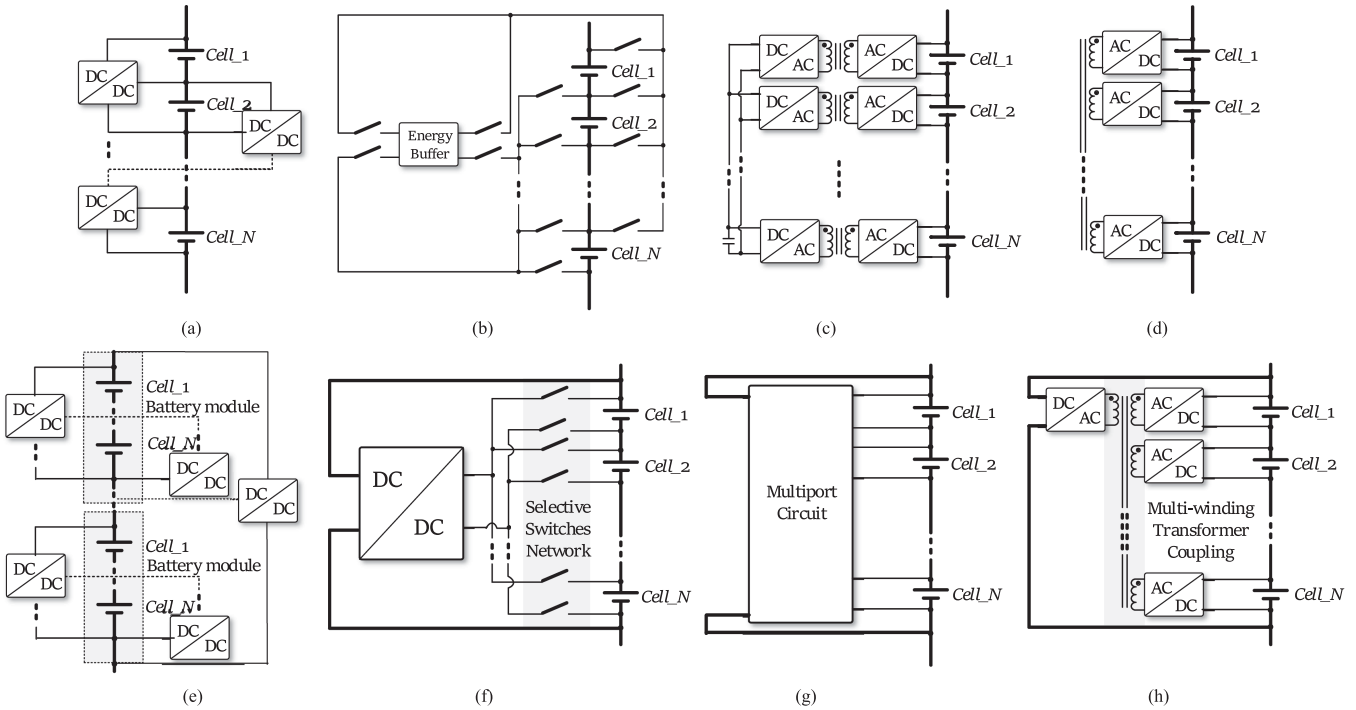

Fig. 2. Block diagrams of a few equalization structures. (a) Adjacent C2C equalizer. (b) EBC2C equalizer. (c) Dc-coupled DC2C equalizer. (d) Multiport-ac-coupled DC2C equalizer. (e) HME. (f) DCSS-based S2C equalizer. (g) MC-based S2C equalizer. (h) Multiwinding transformer coupling-based S2C equalizer.

can only transfer charges to its adjacent battery, and the battery that needs to be equalized can only obtain charges from the adjacent cell. This leads to a decrease in the equalization efficiency as the distance between two cells for equalization increases [27]. In Fig. 2(b), EBC2C uses a shared energy buffer and uses a switching network to select two target battery cells. The energy buffer can be built with inductors, capacitors, *LC* networks, and batteries. The charged battery will initially pass charges to the energy buffer, which will subsequently transfer these charges to the target battery. This structure can transfer charges between any two cells without considering their positions in the battery pack. However, the equalization speed is limited by the energy buffer, and numerous high-frequency switches are required [28].

In Fig. 2(c), dc-coupled C2C equalizer utilizes two "dc–ac–dc" conversion stages to transfer energy between any two arbitrary battery cells, but the equalizer can only select two cells to perform equalization concurrently. Thus, the equalization process must be performed sequentially on an individual cell-by-cell basis and the overall equalization time is prolonged [29]. During equalization, it requires going through four power conversion stages. In Fig. 2(d), multiport-ac-coupled C2C equalizer can process differential power between two battery cells through a "dc–ac–dc" conversion stage. However, similar to the dc-coupled circuit, the equalizer can only equalize two battery cells concurrently and each battery cell requires a half bridge. The number of high-frequency switches is twice the number of the battery cells [30].

In Fig. 2(e), HME structure utilizes multistage dc/dc converters to achieve intra- and intermodule equalizations. This structure has the merits of flexible charge flow path and low component count. However, due to the requirement for two converters to operate synchronously in a multistage structure, its control complexity is a challenge [31]. In Fig. 2(f), the structure of dc–dc converter with selective switches (DCSSs) is simple as it leverages existing dc–dc converters and multiplexer, resulting in a straightforward implementation. However, it typically requires many switches to facilitate the selection of the target batteries. The requirement imposes a demand for intricate control and driving circuits, particularly when equalizing a considerable quantity of batteries. In addition, the DCSS has a single output only. There is a challenge if several batteries need to be equalized. The selector switches are used to select the target battery, and only one battery is equalized at any time [32]. In Fig. 2(g), a multiport converter that replaces converters and selector switches is proposed. Charges can be transferred between target batteries, thus, reducing the number of active devices. The multiport circuit (MC) enables concurrent equalization of multiple batteries, shortening the equalization duration. Multiwinding transformers are commonly used in the MC, as shown in Fig. 2(h). Each transformer winding is introduced for each battery cell. Thus, the presence of numerous cells poses challenges in the design and implementation of the transformer [33].

To reduce the number of active components, alleviate the implementation challenges caused by multiwinding transformers, and enhance the adaptability of the equalizer in systems with different numbers of batteries, a modular-based capacitively coupled equalizer, as shown in Fig. 3, is presented. Such autonomous battery equalization module (ABEM) ("module") exhibit the following characteristics.

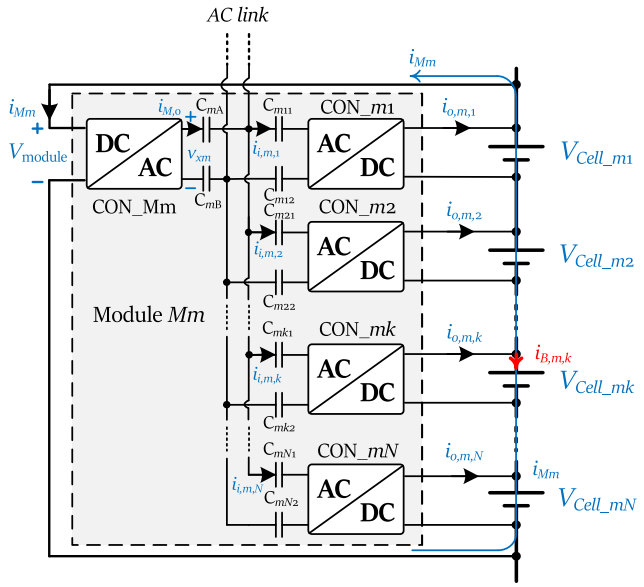

Fig. 3. Structure of the proposed ABEM.

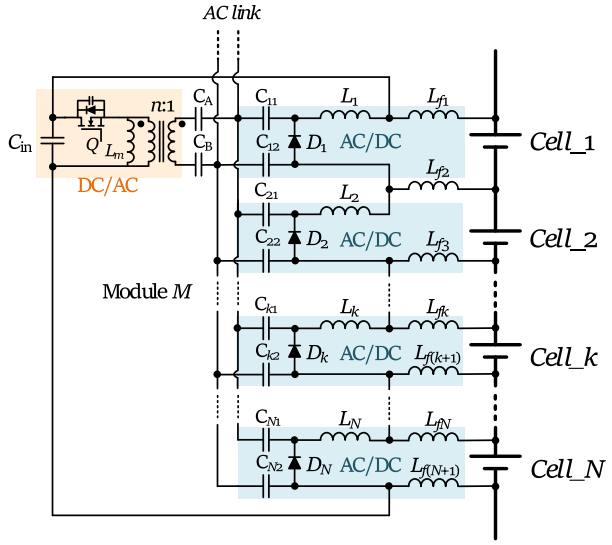

Fig. 4. Schematic of the proposed autonomous voltage balancing circuit module.

1) Each module only requires one switching device. The control circuit is thus simple.
2) Each module requires only one coupled inductors.
3) No selector switches are required. The charging and discharging currents are autonomously distributed.
4) The switching device is operated at a fixed duty cycle and switching frequency.
5) As the SOH is adversely affected by alternating current during equalization [34], [35], the proposed equalizer offers nonpulsating charging or discharging current with small ripple current.
6) The proposed modular structure enables the equalization process to be carried out either within a module or module-to-module.

The rest of this article is organized as follows. Section II outlines the circuit configuration and operational principles. Section III gives the design methodology and power loss analysis. The experimental results of two four-cell modules for equalizing eight 3.6 V, 18 650 batteries are given in Section IV. Section V will address system characteristics and implementation challenges. Section VI will provide a comparative analysis between the proposed method and existing approaches. Finally, Section VII concludes this article.

II. Proposed Equalizer and Operation Principles

As shown in Fig. 3, the proposed module is an S2C structure. A string of N series-connected battery cells is connected to the input of a dc/ac converter that generates a high-frequency voltage to create an ac link via two coupling capacitors. There are totally N ac/dc cell circuits connected in an input-parallel-output-series (IPOS) structure, with their inputs connected to the ac link commonly via two coupling capacitors and their outputs connected to individual cells. Fig. 4 shows the detailed circuit schematic. As illustrated in Fig. 5, for a large-scale system with multiple modules, all modules are connected together via the ac link. In Fig. 4, the dc/ac converter is formed by the switching device Q and the inductor L_m. Its input is connected to the two ends of the battery string formed by the battery cells Cell_1, Cell_2, ..., Cell_N. Its output is connected to the ac link via the capacitors C_A and C_B for decoupling dc component from the output of the dc/ac converter. The input of each ac/dc cell circuit is connected to the ac link via coupling capacitors, C_{11}, C_{12}, C_{21}, C_{22}, ..., C_{k1}, C_{k2}, ..., C_{N1}, C_{N2}, to decouple dc component on the ac link and thus avoid circulating dc current among the cell circuits. Each cell circuit establishes the charging or discharging status of the battery cell it is linked to. Thus, the entire configuration resembles a ZETA converter with multiple outputs [36]. The circuit operates in discontinuous conduction mode or boundary conduction mode (BCM), where the current through L_m reaches zero every switching cycle. The duty cycle of Q is determined by the ratio between the string voltage and the cell voltage. A coupled inductors with a turns ratio of $n:1$ is employed to achieve the required voltage ratio.

A. System Architecture

As exemplified in Fig. 5, the equalizer comprises K modules, shared with the same ac link. Each module has N cells. The architecture facilitates equalization within individual module or across modules. Each battery cell can be discharged to or charged by other battery cells within the same module or other modules. Thus, all battery cells can perform equalization concurrently. All switching devices are designed to be zero-voltage-switched. The voltage stress of all switching devices does not change with the number of modules. Among all coupling capacitors, the capacitors C_{111}, C_{112}, C_{KN1}, and C_{KN2} have the highest voltage stress, which is half the voltage of the whole battery string.

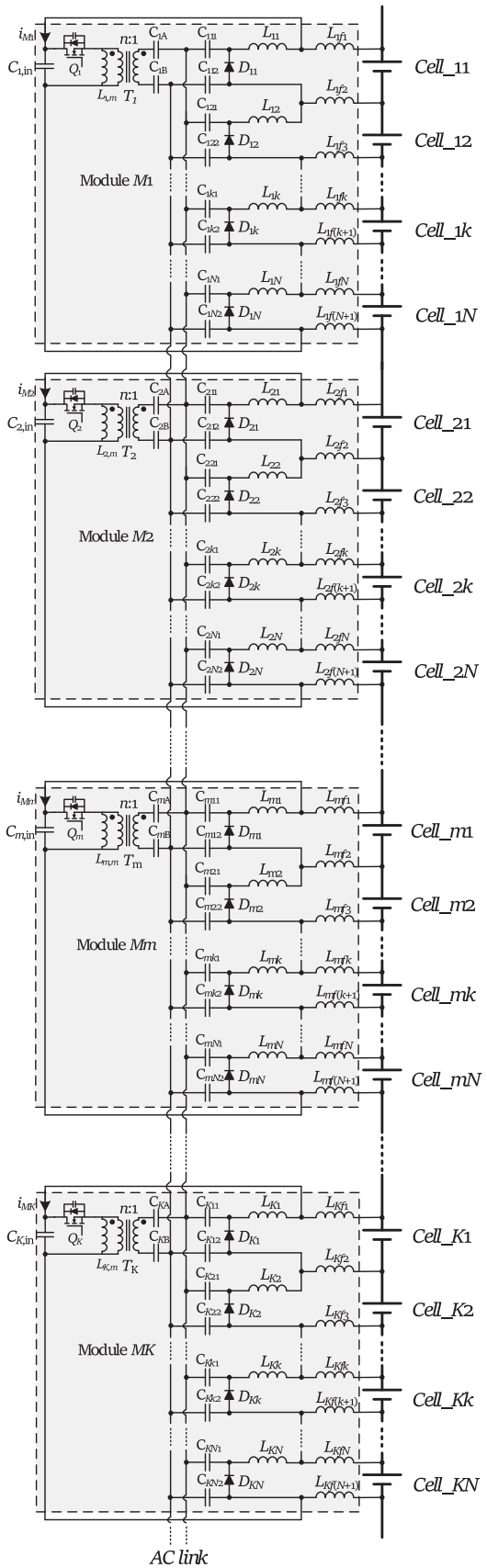

Fig. 5. Circuit schematic of the proposed equalizer using K modules.

B. Operational Principles

For the sake of simplicity and clarity, all components are assumed to be ideal in describing the operating principle of the equalizer. A generic module m is shown in Fig. 3. The module voltage can be expressed as

$$V_{\text{module}} = V_{\text{Cell\_}m1} + \cdots + V_{\text{Cell\_}mN} = \sum_{k=1}^{N} V_{\text{Cell\_}mk}. \quad (1)$$

The dc/ac converter, CON_Mm, generates an ac output v_{xm}. Its amplitude V_{xm} can be expressed as

$$V_{xm} = \frac{\sum_{k=1}^{N} V_{\text{Cell\_}mk}}{n} \quad (2)$$

where n is voltage ratio of CON_Mm. All ac/dc cell circuits, i.e., CON_$m1$ to CON_mN, have their inputs connected in parallel. Thus

$$i_{M,o} = n i_{Mm} = i_{i,m,1} + \cdots + i_{i,m,N} = \sum_{k=1}^{N} i_{i,m,k}. \quad (3)$$

For each ac/dc converter

$$V_{mx} i_{i,m,k} = i_{o,m,k} V_{\text{Cell\_}mk}. \quad (4)$$

Based on (2)–(4), the output current of the cell circuit is

$$i_{o,m,k} = \frac{\sum_{k=1}^{N} V_{\text{Cell\_}mk}}{n V_{\text{Cell\_}mk}} i_{i,m,k}. \quad (5)$$

The equalization current for each battery cell is

$$i_{B,m,k} = i_{o,m,k} - i_{Mm}. \quad (6)$$

According to (5) and (6), the power for equalizing each battery cell can be expressed as

$$V_{\text{Cell\_}mk} i_{B,m,k} = \frac{\sum_{k=1}^{N} V_{\text{Cell\_}mk}}{n} i_{i,m,k} - V_{\text{Cell\_}mk} i_{Mm}. \quad (7)$$

During equalization, the output power equals the input power for the battery string. Therefore

$$V_{\text{Cell\_}m1} i_{B,m,1} + \cdots + V_{\text{Cell\_}mk} i_{B,m,k} + V_{\text{Cell\_}mN} i_{B,m,N} = 0 \quad (8)$$

$$\frac{\sum_{k=1}^{N} V_{\text{Cell\_}mk} \sum_{k=1}^{N} i_{i,m,k}}{n} = i_{Mm} \sum_{k=1}^{N} V_{\text{Cell\_}mk}. \quad (9)$$

Based on (7), the equalization current can be expressed as

$$i_{B,m,k} = \frac{\sum_{k=1}^{N} V_{\text{Cell\_}mk}}{n V_{\text{Cell\_}mk}} i_{i,m,k} - \frac{1}{n} \sum_{k=1}^{N} i_{i,m,k}. \quad (10)$$

Equation (10) can be expressed in a general form of

$$\mathbf{i_{B,m,k}} = \mathbf{A i_{i,m,k}} \quad (11)$$

where

$$\mathbf{i_{B,m,k}} = \begin{bmatrix} i_{B,m,1} & i_{B,m,2} & \cdots & i_{B,m,N} \end{bmatrix}^T$$

$$\mathbf{i_{i,m,k}} = \begin{bmatrix} i_{i,m,1} & i_{i,m,2} & \cdots & i_{i,m,N} \end{bmatrix}^T$$

and

$$\mathbf{A} = \begin{bmatrix} \frac{\sum_{k=1}^{N} V_{\text{Cell\_}mk}}{nV_{\text{Cell\_}m1}} - \frac{1}{n} & -\frac{1}{n} & \cdots & -\frac{1}{n} \\ -\frac{1}{n} & \frac{\sum_{k=1}^{N} V_{\text{Cell\_}mk}}{nV_{\text{Cell\_}mk}} - \frac{1}{n} & \cdots & -\frac{1}{n} \\ \vdots & \vdots & \ddots & \vdots \\ -\frac{1}{n} & -\frac{1}{n} & \cdots & \frac{\sum_{k=1}^{N} V_{\text{Cell\_}mk}}{nV_{\text{Cell\_}mN}} - \frac{1}{n} \end{bmatrix}.$$

The input current of the cell circuit, $\mathbf{i_{i,m,k}}$ can be calculated by considering the input impedance of the circuit.

C. Circuit Operation of the ABEM

The ABEM has two operating modes in every switching cycle. Fig. 6(a) shows the first operating mode when Q_m is ON. Fig. 6(b) shows the second operating mode when Q_m is OFF. Fig. 7 shows the key waveforms. Fig. 8(a) shows the simplified circuit for describing the two-stage converter. Fig. 8(b) shows the equivalent circuit when the main switch is turned-ON. Fig. 8(c) shows the equivalent circuit for the charging cells when the main switch is turned-OFF. For the sake of simplicity, the filter inductor is neglected in the analysis. Due to the variation of the initial cell voltages, the ac/dc cell circuits operate differently. Considering the scenario that Cell_$m1$ is discharged, and Cell_$m2$ is charged. During the "ON" period (T_{on}), as illustrated in Fig. 6(a) and 7, the switch is turned on, causing the current through the output inductor L_{m2} to increase, and the current through the output inductor L_{m1} to reduce to zero and then increase. All diodes are OFFwhen Q_m is turned-ON. During the "OFF" period (T_{off}), as illustrated in Fig. 7, the switch is turned-OFF, causing the current of the output inductor L_{m2} to reduce, and the current of the output inductor L_{m1} to reduce to zero and then increase. Only the diodes (e.g., D_{m2}) corresponding to the batteries that require charging are conducting, while the diodes associated with the higher voltage batteries remain OFF.

The whole battery string provides the input voltage for the single module. The input current of the module equals the current flowing out of the battery string. When the battery cell voltage is higher than the average voltage of the battery string, the diode in the ac/dc cell circuit connected to the battery cell will be blocked, and the average current of L_{mk} ($i_{o,m,k}$) is zero, implying that the average current flowing from the ac/dc cell circuit to the battery cell is zero, and the discharging current of the battery cell is i_{Mm}. The battery cell of the lowest voltage will be charged. The equalization process operates autonomously, with the equalization current diminishing as the voltage difference decreases. When the voltage difference between batteries approaches zero, the equalization current also reduces to zero.

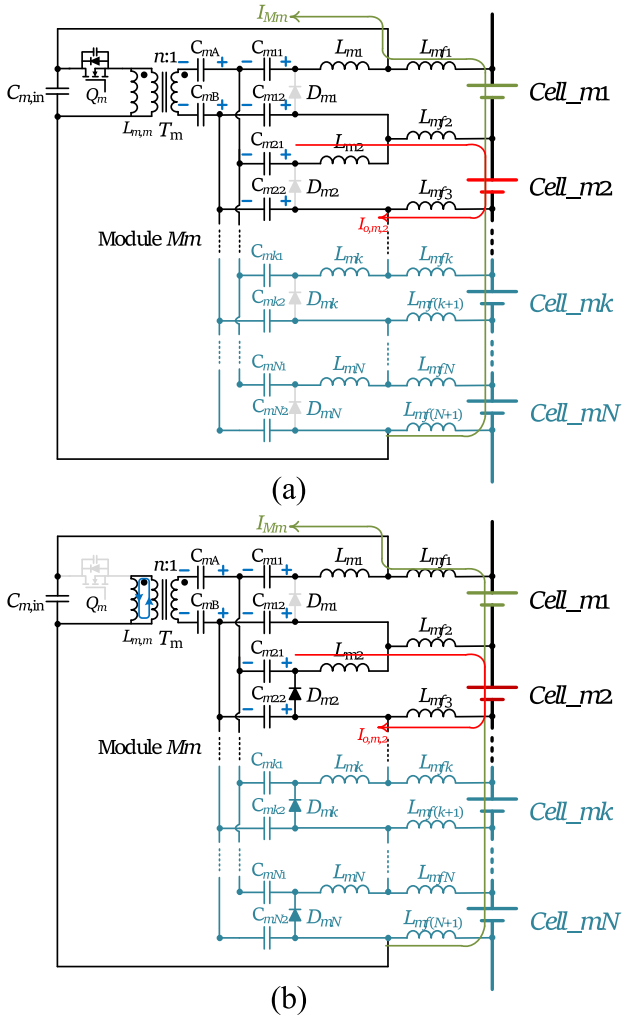

Fig. 6. Topological operation of the ABEM. (a) Q_m is ON. (b) Q_m is OFF.

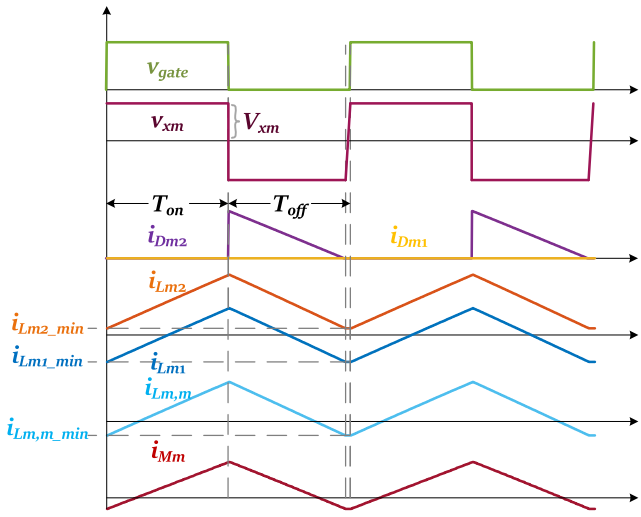

Fig. 7. Key waveforms in the steady state during balancing.

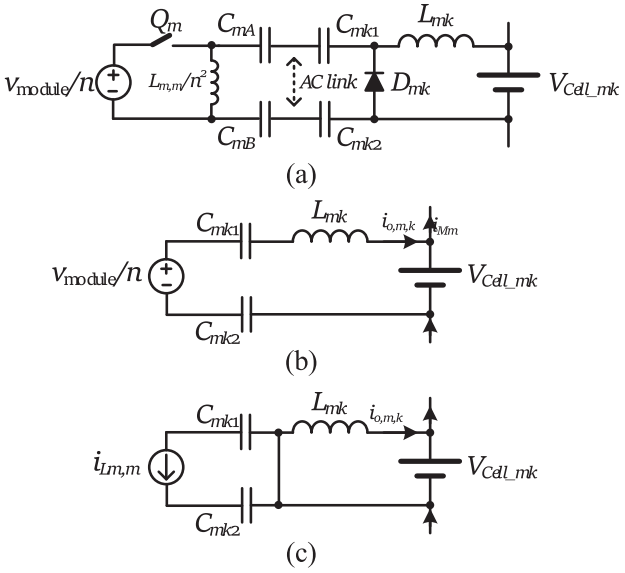

Fig. 8. Equivalent circuits. (a) Simplified circuit of the converter. (b) Equivalent circuit of the cell circuit for all cells when switches are turned-ON. (c) Equivalent circuit of the cell circuit for the charging cells when switches are turned-OFF.

D. Analysis of Equalization Current

When the switch is turned-ON, as shown in Fig. 6(a), the magnetizing inductance, $L_{m,m}$, of the coupled inductors is charged. The voltage across $L_{m,m}$ is

$$V_{Lm,m} = V_{\text{module}}. \tag{12}$$

The output inductor voltage can be expressed as

$$\begin{cases} V_{Lm1} = \dfrac{\sum_{k=1}^{N} V_{\text{Cell\_}mk}}{n} + V_{Cm1} - V_{Cm2} - V_{\text{Cell\_}m1} \\ \qquad +V_{CmA} - V_{CmB} \\ V_{Lm2} = \dfrac{\sum_{k=1}^{N} V_{\text{Cell\_}mk}}{n} + V_{Cm3} - V_{Cm4} - V_{\text{Cell\_}m2} \\ \qquad +V_{CmA} - V_{CmB} \\ \vdots \\ V_{Lmk} = \dfrac{\sum_{k=1}^{N} V_{\text{Cell\_}mk}}{n} + V_{Cm(2k-1)} - V_{Cm2k} - V_{\text{Cell\_}mk} \\ \qquad +V_{CmA} - V_{CmB}. \end{cases} \tag{13}$$

All diodes are turned-OFF and the currents of the coupling capacitors are

$$\begin{cases} i_{Cm1} = -i_{Lm1} \\ i_{Cm3} = -i_{Lm2} \\ \vdots \\ i_{Cm(2k-1)} = -i_{Lmk}. \end{cases} \tag{14}$$

When the switch is turned-OFF, the charging circuit and discharging circuit have different operating modes, as shown in Fig. 6(b), $L_{m,m}$ is being discharged. The voltage across $L_{m,m}$ is

$$\begin{aligned} V_{Lm,m} &= -n\left(V_{Cm3} - V_{Cm4} + V_{CmA} - V_{CmB}\right) \\ &= n(-V_{Cm1} + V_{Cm2} + V_{Lm1} + V_{\text{Cell\_}m1} \\ &\quad + V_{CmA} - V_{CmB}). \end{aligned} \tag{15}$$

At this time, the diode D_{m2} in the circuit of the battery with the lowest voltage is turned-ON first. The voltage of the ac link is clamped, and the other diodes (e.g., D_{m1}) are turned-OFF. V_{Lm1} and V_{Lm2} can be expressed as

$$V_{Lm1} = -V_{\text{Cell\_}m1} + V_{Cm1} - V_{Cm2} + \frac{V_{Lm,m}}{n} - V_{CmA} + V_{CmB} \tag{16}$$

$$V_{Lm2} = -V_{\text{Cell\_}m2}. \tag{17}$$

Moreover, all capacitor currents can be expressed as

$$i_{Cm1} = -i_{Lm1} \tag{18}$$

$$i_{Cm1} + i_{Cm3} + \cdots + i_{Cm(2k-1)} = n i_{Lm,m}. \tag{19}$$

Since the circuit operates at BCM, the period of time during which the currents of the output inductors, $L_{m1} \sim L_{mk}$, remain constant can be neglected. Equation (20) shown at the bottom of the next page, illustrates the principle of capacitor amp-second balance of C_{m3}, where D is the duty cycle of the switch, and $I_{Lm1\_\min}$ and $I_{Lm2\_\min}$ are minimum currents of inductors L_{m1} and L_{m2}, respectively. According to KCL According to KCL

$$I_{Lm1\_\min} + I_{Lm2\_\min} = -nI_{Lm,m\_\min}. \tag{21}$$

During equalization, it is assumed that the current of a batteries is discharged and the current of b batteries is charged. Equation (21) can be expressed as

$$aI_{Lm1\_\min} + bI_{Lm2\_\min} = -nI_{Lm,m\_\min}. \tag{22}$$

By using (19), (20), and (22), the minimum current of L_{m2} can be shown to be

$$\begin{aligned} I_{Lm2\_\min} = a&\frac{\sum_{k=1}^{N} V_{\text{Cell\_}mk}}{2nL}(1-D)^2 T_s \\ &+ \frac{n\sum_{k=1}^{N} V_{\text{Cell\_}mk}}{2L_{m,m}} D\,(1-D)\,T_s \\ &- \frac{V_{\text{Cell\_}m2}}{2L} D\,(1-D)\,T_s \end{aligned} \tag{23}$$

where $L = L_{m1} = L_{m2}$. Similarly, according to capacitor C_{m1} amp–second balance, the minimum current of L_{m1} can be derived as

$$I_{Lm1\_\min} = -\frac{\sum_{k=1}^{N} V_{\text{Cell\_}mk}}{2nL}(1-D)T_s. \tag{24}$$

The average current of the output inductor L_{m2} can be calculated as

$$I_{Lm2} = \frac{V_{\text{Cell\_}m2}}{2L}(1-D)T_s + I_{Lm2\_\min}. \tag{25}$$

The average current of $L_{m,m}$ is the discharging current of the battery string during equalization. It can be shown that

$$I_{Mm} = \frac{D^2 T_s \sum_{k=1}^{N} V_{\text{Cell\_}mk}}{2} \left(\frac{1}{L_{m,m}} + \frac{N}{n^2 L} \right). \tag{26}$$

The equalization current can be calculated by (6), (25), and (26).

III. Design Methodology

A. Design Consideration

The equalization currents in charging and discharging are analyzed in Section II-C. During the equalization process, the equalization current gradually decreases until the voltage difference between the batteries is eliminated. Consequently, the initial value of the equalization current can only be calculated based on the initial voltage distribution. From (25) and (26), it is found that the equalization current is not only influenced by the duty cycle and voltage distribution, but also significantly affected by the inductance value. A higher current can achieve faster equalization, but the presence of diodes leads to increased conduction losses. In addition, the voltage ripple of the coupling capacitors also affect equalization speed and efficiency. The relationship between the component values and losses is studied. In addition, the design of the coupled inductors needs to take into account the number of batteries. Zero-voltage-switching (ZVS) of the switch is considered.

B. Loss Analysis

There are three primary sources of loss in the equalizer. They are switching and conductor losses of the switching devices, $Q_1 \sim Q_K$, conduction losses of the diodes, $D_{11} \sim D_{KN}$, and the magnetic components, $L_{11} \sim L_{KN}$ and $T_1 \sim T_K$. As $Q_1 \sim Q_K$ are turned-ON at zero voltage, their turn-ON power losses are ignored. Their major switching losses occur at turn-OFF. Thus, the overall turn-OFF loss P_{off} and the conduction loss P_{con} are

$$P_{\text{off}} = \left[\frac{1}{2} \sum_{k=1}^{N} V_{\text{Cell\_}mk} I_{\text{off}} T_f - \frac{1}{2} C_{\text{oss}} \left(\sum_{k=1}^{N} V_{\text{Cell\_}mk} \right)^2 \right] f_s \tag{27}$$

$$P_{\text{con}} = R_{\text{on}} I_{Mm}^2 \tag{28}$$

where I_{off} is the current of the switching device at turn-OFF, T_f is the turn-OFF time obtained from the datasheet, R_{on} is the ON-state resistance of the switching device, and I_{Mm} is the rms current of the input current.

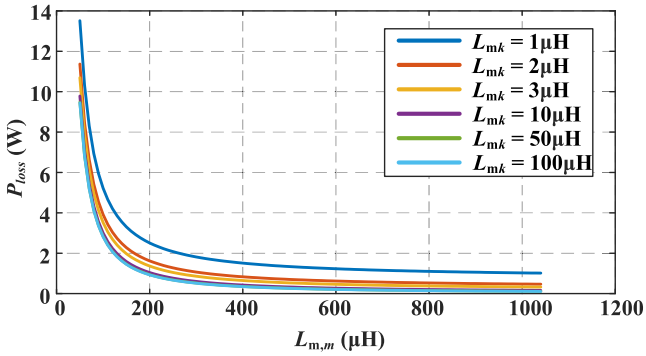

Fig. 9. Power loss versus magnetizing inductance ($L_{m,m}$).

Thus, the total loss of the switching device loss P_{sw} is

$$P_{\text{sw}} = P_{\text{off}} + P_{\text{con}}. \tag{29}$$

The diode loss P_{diode} equals

$$P_{\text{diode}} = J \cdot V_D \frac{V_{\text{Cell\_}mk}}{2L} (1-D)^2 T_s \tag{30}$$

where J is the number of the cells under charging and V_D is the forward voltage of the diodes.

The coil loss of the magnetic components P_{coil} is expressed as

$$P_{\text{winding}} = R_{\text{coup}L\_\text{winding}} {I_{Mm}}^2 + R_{L\_\text{winding}} {I_{Lmk}}^2 N + R_{Lf\_\text{winding}} {I_{Lmfk}}^2 (N+1) \tag{31}$$

where $R_{\text{coup}L\_\text{winding}}$ is the dc resistance of the coil in coupled inductors, R_{L_winding} and R_{Lf_winding} are the dc resistance of inductors ($L_{m1} \sim L_{mN}$) and ($L_{mf1} \sim L_{mf(N+1)}$), respectively, and I_{Lmk} is the rms current of inductors ($L_{m1} \sim L_{mN}$).

Thus, the total loss of the system P_{loss} is

$$P_{\text{loss}} = K \left(P_{\text{sw}} + P_{\text{diode}} + P_{\text{winding}} \right) \tag{32}$$

where K is the number of the modules.

The total loss versus magnetizing inductance ($L_{m,m}$) is depicted in Fig. 9. When $L_{m,m} > 200\mu$H, the loss significantly drops. In addition, when the inductance $L_{m,k} > 10\mu$H, the reduction in loss becomes insignificant. In circuit design, tradeoffs need to be made among conduction losses, switching speed, and component size.

C. Voltage Stress of Coupling Capacitors

The voltage stress of coupling capacitors is derived. To simplify the analysis, the effects of the diodes and inductors are

$$- \left(\frac{V_{\text{Cell\_}m2}}{2L_2} (1-D) T_s + I_{L\_m2\_\min} \right) D + \left[n \left(\frac{\sum_{k=1}^{N} V_{\text{Cell\_}mk}}{2L_{m,m}} D T_s + I_{Lm,m\_\min} \right) + \left(\frac{\sum_{k=1}^{N} V_{\text{Cell\_}mk}}{2nL_{m1}} (1-D) T_s + I_{Lm1\_\min} \right) \right] (1-D) = 0. \tag{20}$$

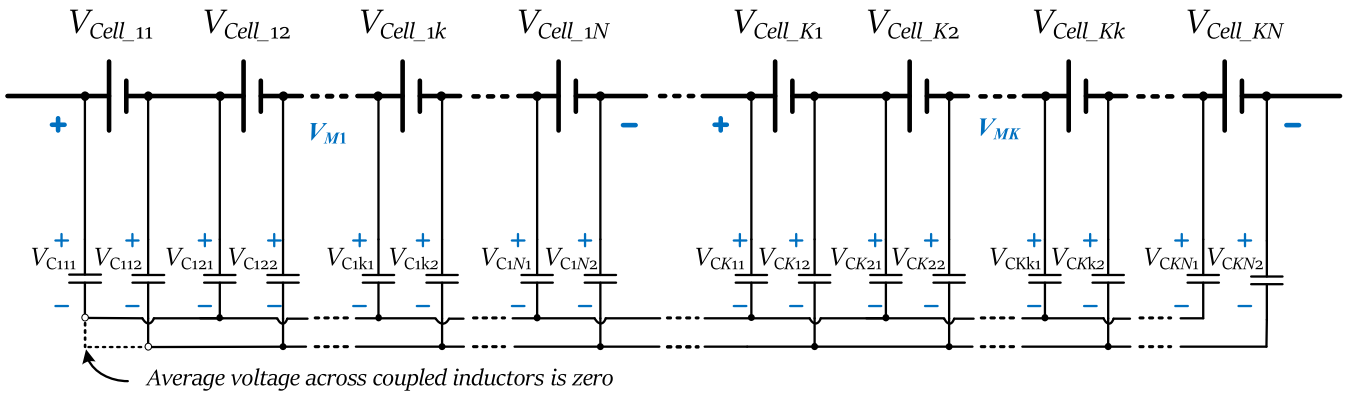

Fig. 10. Simplified circuit for capacitor voltage stress analysis.

ignored. As shown in Fig. 10, the capacitors with the maximum voltage stress are C_{111}, and C_{KN2}, their voltage stresses can be expressed as

$$V_{C111} = -V_{CKN2} = \frac{1}{2}\sum_{m=1}^{K} V_{Mm}. \tag{33}$$

The relationship between the voltage stress of the coupling capacitors is

$$V_{CKk1} = V_{CK(k+1)1} - V_{\text{Cell\_}Kk} = V_{CK(k-1)1} + V_{\text{Cell\_}K(k-1)} \tag{34}$$

where the voltage variables defined in (34) are shown in Fig. 10.

The capacitors situated at the extremities will endure the highest voltage stress, while those closer to the center experience comparatively lower voltage stress. The maximum capacitor voltage stress equals one half of the string voltage. In other words, the maximum number of modules is determined by the voltage rating of the coupling capacitors.

D. Voltage Spike Suppression and ZVS Analysis

Due to the nonideal nature of the coupled inductors in the experimental setup, the effect of the leakage inductance is studied. The nonideal model of the dc/ac converter is depicted in Fig. 11(a). As shown in Fig. 11(b), the leakage inductance results in the occurrence of voltage spikes upon switching OFF the switching device Q. The spike voltage V_{spike} is

$$V_{\text{spike}} = L_g \frac{di}{dt}. \tag{35}$$

The high voltage spike resulting from the sudden drop of current to zero can potentially damage the MOSFET. Therefore, it is necessary to design the drain-source capacitance C_{mos} to suppress the voltage spike.

ZVS is achieved via a quasiresonance operation. Upon the diodes turning OFF [as marked in Fig. 11(b)], the input circuit starts resonating. Fig. 11(c) shows the equivalent circuit with all battery cells modeled as short circuit. The equivalent inductance L_e and capacitance C_e on the secondary side of the coupled

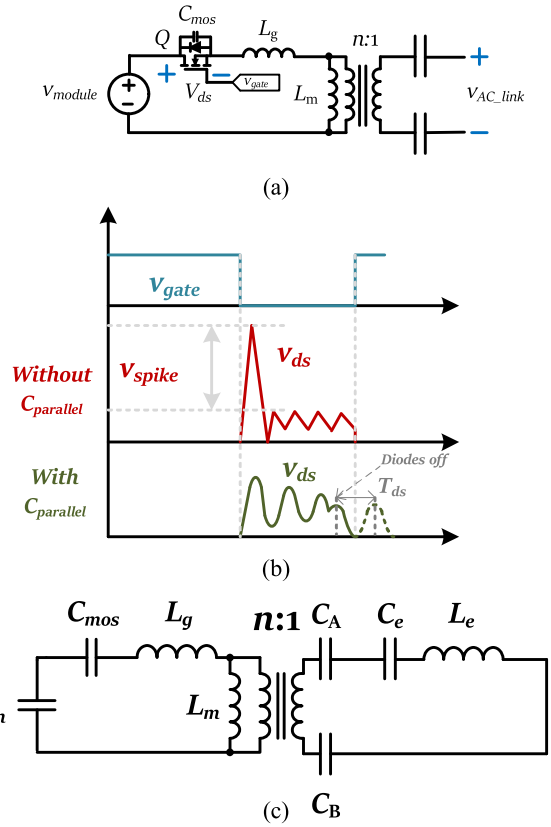

Fig. 11. (a) Nonideal model of the dc/ac converter. (b) V_{gate} and V_{ds} of the switch Q. (c) Equivalent circuit for ac analysis.

inductor are

$$\begin{cases} L_e &= \frac{L_{mk}}{N} \\ C_e &= \frac{N}{2} C_{mk}. \end{cases} \tag{36}$$

The equivalent impedance Z_e on the primary side of the coupled inductor is

$$Z_e = n^2 \left(j\omega L_e + \frac{1}{j\omega C_e} + \frac{1}{j\omega C_A} + \frac{1}{j\omega C_B} \right) \parallel j\omega L_m + j\omega L_g + \frac{1}{j\omega C_{\text{mos}}}. \tag{37}$$

The value of C_{mos} is designed to make the switch turn-ON again when v_{ds} resonates to 0V with the resonant period of T_{ds}. It can be shown that T_{ds} is

$$T_{ds} = \frac{2\pi\sqrt{2a}}{\sqrt{-b+\sqrt{b^2-4ac}}} \tag{38}$$

where

$$\begin{aligned} a =& \, n^2 C_{\text{oss}} L_m L_g L_e C_e C_A C_B \\ &+ n^2 C_{\text{oss}} (L_g L_e C_e C_A C_B + L_e L_m C_e C_A C_B) \\ b =& \, -[n^2 C_{\text{oss}} L_g (C_A C_B + C_A C_e + C_B C_e) \\ &+ L_m C_e C_A C_B + n^2 L_e C_e C_A C_B \\ &+ n^2 C_{\text{oss}} L_m (C_A C_B + C_A C_e + C_B C_e)] \\ c =& \, n^2 (C_A C_B + C_A C_e + C_B C_e). \end{aligned} \tag{39}$$

Detailed derivation of T_{ds} is given in the Appendix.

The value of C_{mos} is

$$C_{\text{mos}} = C_{\text{oss}} + C_{\text{parallel}} \tag{40}$$

where C_{oss} is the parasitic capacitance and C_{parallel} is the additional capacitance connected in parallel with the switch to help adjust the T_{ds} to achieve ZVS.

The value of C_{parallel} is chosen to be much larger than C_{oss}. Thus, the value of C_{mos} is dominated by the value of C_{parallel}. Thus

$$C_{\text{mos}} \approx C_{\text{parallel}}. \tag{41}$$

The resonance operation is then less affected by the variance of the device output capacitance.

IV. Experimental Verification

A. Experimental Setup

A laboratory prototype comprising two ABEMs—Modules 1 and 2—has been constructed and evaluated. It is shown in Fig. 12(a). The setup accommodates eight series-connected batteries grouped into two sets, with one set connected to Module 1 and the other to Module 2, employing retired 2600 mAh Samsung ICR18650 lithium-ion batteries. Circuit parameters are given in Table I, with the controller STM32F407 in use. The coupled inductor has a turns ratio of $4.5:1$. A cell circuit is shown in Fig. 12(b). To optimize the conversion efficiency of the modular equalizer, low forward voltage power Schottky diodes (30BQ015) have been incorporated. Battery voltages are recorded using a Keysight 34 970 A data logger.

B. Experimental Results

Fig. 13 shows the key waveforms in Modules 1 and 2. Fig. 13(a) shows the waveforms of the gate-source voltages, v_{gs1} and v_{gs2}, and the drain-source voltages, v_{ds1} and v_{ds2}, of the MOSFETs in Modules 1 and 2, respectively. Each MOSFET has a 1000 pF capacitor connected across its drain and source. It can be observed that both MOSFETs are switched on and off at zero voltage. Fig. 13(b) shows the inductor current (i_{L1}), module input current (i_M), filter inductor current (i_{Lf1}), and ac link voltage. As shown in Figs. 13(c), the inductors exhibit varying dc biases, due to variations in battery voltage.

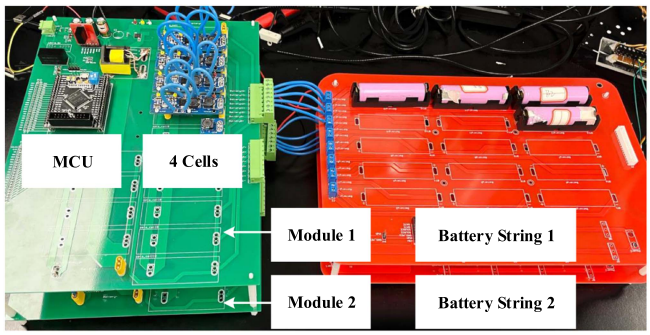

(a)

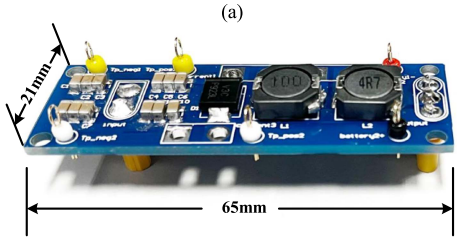

(b)

Fig. 12. (a) Experimental setup with two modules. (b) Designed ac/dc balancing circuit prototype.

TABLE I
Critical Design Parameters

Component Type	Parameters
Microcontroller	STM32F407
MOSFET(Q_m)	BSC320N20N
Battery	ICR18650
Diode(D_m)	30BQ015 SCHOTTKY
Coupled inductor turns ratio (n)	$4.5:1$
Magnetizing inductance ($L_{m,m}$) (n)	$220\mu H$
Switching frequency (f_s)	200kHz
Coupling capacitor ($C_{mA}/C_{mB}/C_{mk}$)	$13\mu F$
Inductor (L_{mk})	$10\mu H$
Filter inductor (L_{mfk})	$4.7\mu H$

Fig. 14 depicts the measured voltage of the four batteries in the experiment. These four batteries are grouped as one battery string, and which is balanced by one equalizer module. Fig. 14(a) shows the equalization result under the static condition for four cells whose initial voltages are about 3.452, 3.442, 3.419, and 3.153 V, respectively. The equalizer reduces the voltage difference from 299 to 18 mV in 4300 s. In Fig. 14(b) and (c), the equalization experiments are conducted with 1 and 2 A charging current. The initial voltage differences are 479 and 229 mV. The voltage difference is lower than 20 mV after equalization. Fig. 14(d) shows the equalization result during the discharging process with a 16Ω load.

In order to further verify the performance of the proposed modular equalizer, the multilevel balancing experimental results

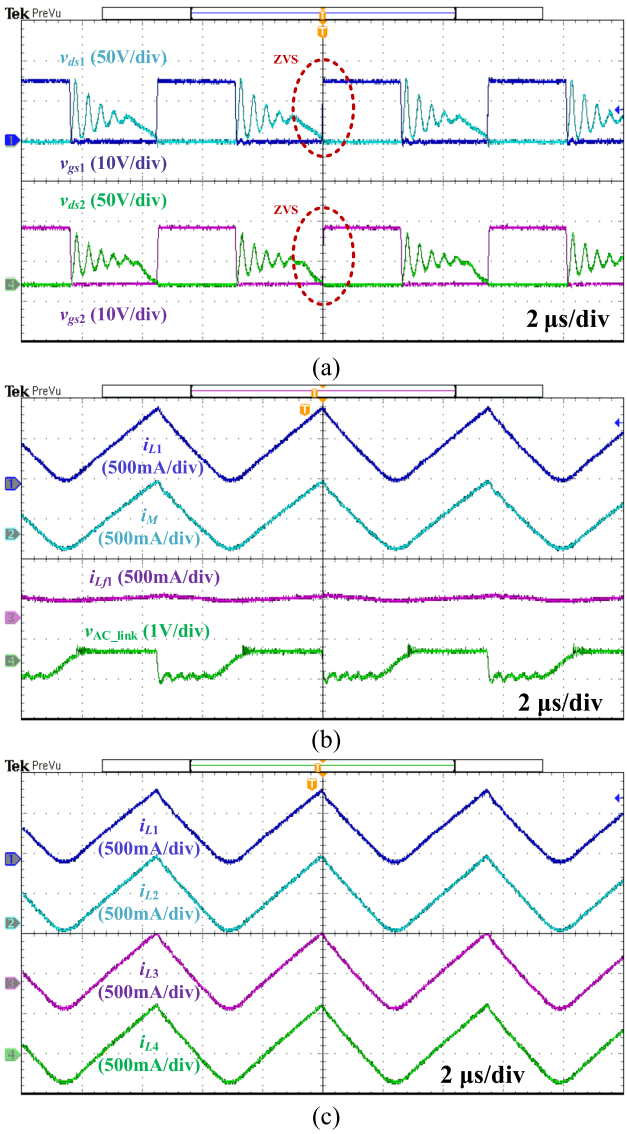

Fig. 13. Key waveforms of the ABEM. (a) Switches Q_1 and Q_2: gate drive signal v_{gs1} and v_{gs2}, drain source voltage v_{ds1} and v_{ds2}. (b) Inductor current i_{L1}, module input current i_M, filter inductor current i_{Lf1}, and ac link voltage $v_{\text{ac\_link}}$. (c) Inductor current $i_{L1}, i_{L2}, i_{L3}, i_{L4}$.

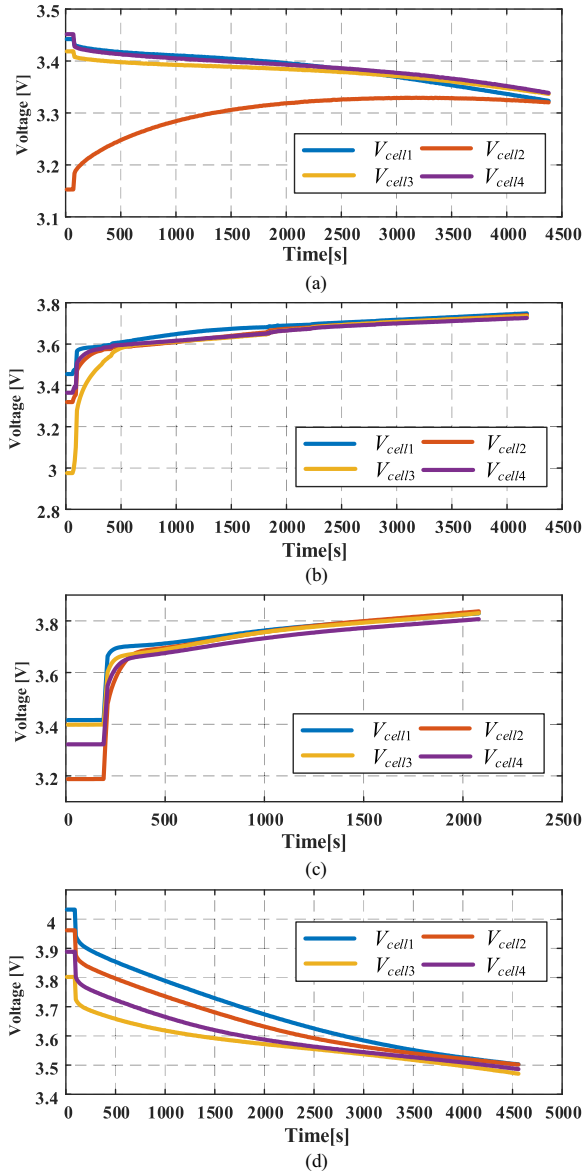

Fig. 14. Experiment results for four cells with different distributions. (a) Idle condition for single module balancing. (b) Charging condition with 1 A current. (c) Charging condition with 2 A current. (d) Discharging condition with a 1616Ω load.

are captured in Fig. 15. Two equalizing circuits are coupled by ac link to balance eight series connected batteries. Moreover, two modules share a controller, and a 200 kHz PWM signal drives two MOSFETs simultaneously. As shown in Fig. 15(a), the modular equalizer reduces the voltage difference from 458 to 20 mV in 3060 s. In Fig. 15(b) and (c), the equalization is conducted with 1A charging current and a 32Ω load, respectively. The maximum voltage difference of the battery string is also lower than 20 and 30 mV after equalization. Fig. 16 shows the theoretical efficiency and measured efficiency versus the cell voltage. As the battery voltage is charged from 3.104 to 3.860 V, the efficiency consistently remains above 85%, with a peak value of 86%.

Fig. 17(a) shows the measured voltage waveforms across the coupling capacitors when there is only one module ($M1$). The total string voltage is 13.2 V and the voltage across the four coupling capacitors are 6.62, 3.35, –0.06, and –3.42 V, respectively. With an added module, Fig. 17(b) shows the waveforms in the same module, i.e., $M1$. The total string voltage with the two modules is 26.5 V and the voltage across the four coupling capacitors are 13.2, 9.94, 6.48, and 3.21 V, respectively. Thus, it can be shown that the voltage stress of the coupling capacitors increases with the number of modules and is aligned with the predicted values given in Section III-C.

V. Discussions

Each module only requires one switching device and has low equalization current. For example, the designed equalization current is less than 600 mA in the prototype and the entire

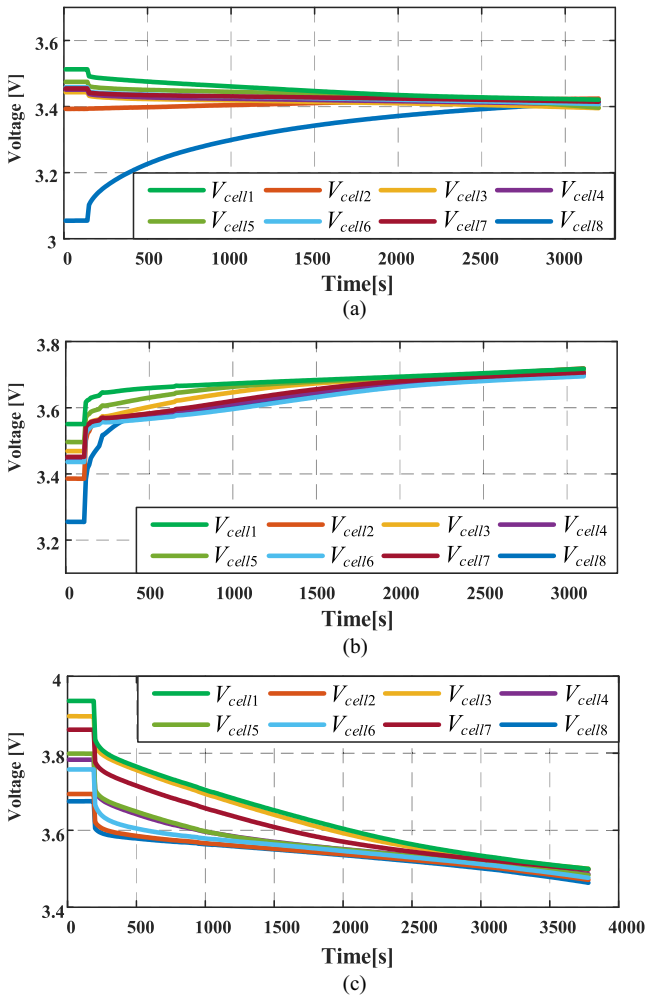

Fig. 15. Experiment results for eight cells with different distributions. (a) Idle condition for two modules balancing. (b) Charging condition with 1 A current. (c) Discharging condition with a 32Ω load.

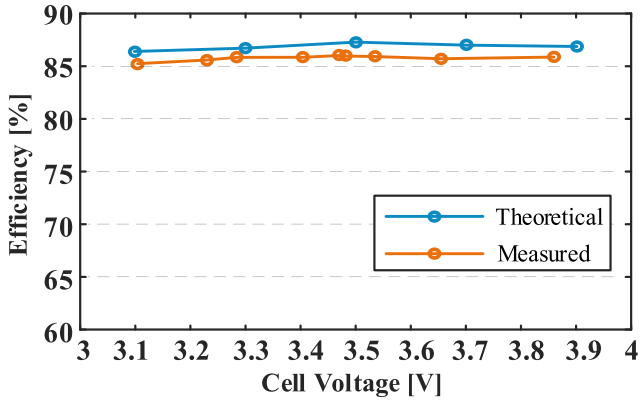

Fig. 16. Theoretical efficiency and measured efficiency against cell voltage.

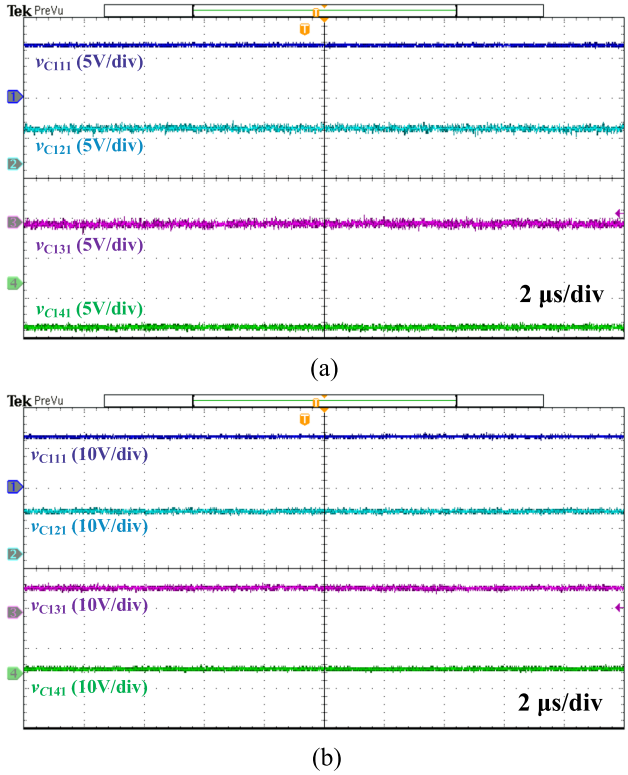

Fig. 17. (a) Voltage stress of one module ($M1$) balancing. (b) Voltage stress of module $M1$ of two modules balancing.

power dissipation is less than 0.2 W. Management of the heat dissipation is not critical. As the equalizer is used to equalize battery cell voltages, no special requirement for coping with the electrochemical characteristics of the batteries is needed.

Considering the nonideal characteristics of the circuit components, such as diode forward voltage, equivalent series resistances (ESRs) of the coupling capacitors and filter inductors, Fig. 18(a) shows the equivalent circuit. The dc/ac converter is modeled by an ac source $v_{\text{ac\_link}}$ supplying to multiple parallel-connected cell circuits via coupling capacitors. Each cell circuit is connected to a battery cell. As the cell circuits can be considered individually, they are combined and modeled by an equivalent circuit shown in Fig. 18(b). Ideally, the final voltage of the equalized battery equals the average voltage of the battery pack.

Based on considering the dc operation, variations, and tolerance of the values of the coupling capacitors and filter inductors do not affect the equalization performance. However, the ESR of the components can cause impact to the performance. First, the voltage drops across the ESRs cause the final voltage of the equalized battery lower than the average voltage of the battery cells. Second, the variation of the ESRs causes the differences in the final battery cell voltages. The forward voltage drop of the diodes can also affect the final battery voltage. As shown in Section III-B, the conduction loss of the diodes is the main source of power dissipation. Hence, coupling capacitors and filter inductors with low ESR and small variation in the ESR, and diodes with low forward voltage drop can enhance equalization performance and efficiency.

Each module requires one gate signal. Thus, as the gate signals to all MOSFETs have to be synchronized to produce the ac link voltage, a gate-signal synchronization, such as daisy-chained

TABLE II
COMPARISON OF THE REQUIRED NUMBER OF COMPONENTS USED IN DIFFERENT EQUALIZERS

Circuit topology	System modularity	External supply source	Number of switches (Ratio of # of gate drivers w.r.t. # of switches)	Ratio of switch voltage stress w.r.t. cell voltage	Selection switches & Drivers	No. of passive components			
						Diode	Capacitor	Inductor	Transformer/ Coupled inductor (windings)
Buck-boost [12]	No	No	$2n$ (1)	1	0	0	n	0	$n/2(n)$
Cuk [13]	No	No	2 (1)	1	n+2(DPDT) +2(SPST)	0	2	2	0
LC network [14]	No	No	$8m+8$ (1)	n	$4n+4m$	0	$m+1$	$m+1$	0
Flyback/forward [37]	No	No	$2n$ ($\frac{1}{2}$)	1	0	0	0	0	1 (n)
Transformer carrier [38]	No	No	$2n+6$ ($\frac{n+5}{2n+6}$)	n	0	0	0	0	1 (2)
LLC & buck-boost [18]	Yes	No	$6m+2$ (1)	n	$m+5$	2	2	$3m$	1 (3)
Class-D & multi-active-bridge [39]	Yes	No	$2n+\frac{n}{2}$ (1)	4	0	0	n	$2n$	$n(1)+\frac{n}{4}(3)$
IRSWVD-SVM [40]	No	No	$2m$ (1)	$\frac{n}{m}$	0	$6n$	$3n$	$3m$	0
LCC converter [21]	No	No	2 (1)	n	$2n$	2	2	1	1 (3)
Stacked buck-boost [22]	No	No	1 (1)	n	0	n	$n+1$	$n+1$	1 (2)
AC-Bus SEPIC [23]	Yes	No	$\frac{n}{2}$ (1)	2	0	n	n	n	$\frac{n}{2}(n)$
Multiport converter [24]	No	No	$4n+4$ (1)	$\frac{n}{2}$	$2n$	0	$2n+1$	$n+1$	1 ($n+1$)
Half-bridge converter [25]	No	No	$n+4$ (1)	$\frac{n}{2}$	0	0	4	1	1 ($n+1$)
Parallel-transformers [26]	No	Yes	1 (1)	n	0	$n+1$	1	0	$\frac{n}{8}(n+\frac{n}{4}+2)$
Proposed structure	Yes	No	m (1)	$\frac{n}{m}$	0	n	$2n+m$	$2n+m$	$m(2m)$

Note: n: number of battery cells. m: number of modules. DPDT: Double pole double throw. SPDT: Single pole double throw.

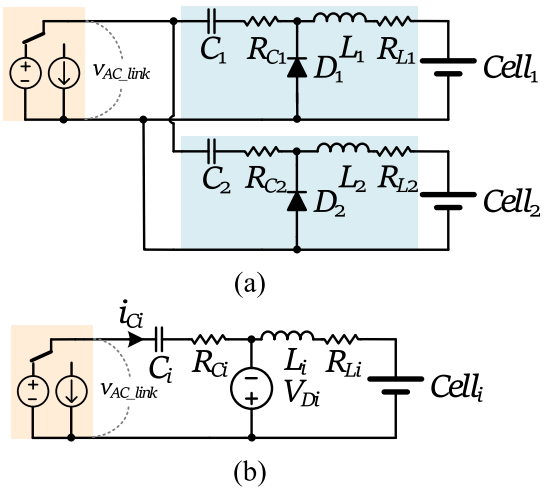

Fig. 18. (a) Equivalent circuit with nonideal components for two cells. (b) Equivalent circuit with nonideal components for one cell.

network, is needed. Further research will be dedicated into the gate-signal synchronization technique.

VI. COMPARISON WITH PRIOR ART

Table II presents a comprehensive comparison between the proposed equalizer and existing solutions based on system modularity, use of external power source, number of switching devices, the ratio of the drivers in relation to the number of switches, passive components, and the ratio of voltage stress on switching devices in relation to the cell voltage. In [12], based on a flux compensation approach, a buck-boost converter-based C2C equalizer that can reduce the number of magnetic devices is proposed. However, each battery requires two MOSFETs, thus, the control will be more complicated, and the cost will increase. In [13], a capacitively level-shifted Cuk-converter-based structure, which utilizes low-frequency selection switches to reduce the cost of the drive circuits, is proposed. However, the power loss, volume, and reliability of the relays need to be considered. In [14], a matrix and half-bridge *LC* converter-based structure, which utilizes switch network to achieve multicells to multicells, is proposed. However, this solution requires numerous selection switches. When the equalization target has multiple batteries, the equalizer requires these batteries to be adjacent. The flexibility is then confined. In [37], a multiwinding transformer structure that realizes any cell to any cell equalization is proposed. However, excessive windings will lead to nonnegligible parasitic parameters, which significantly reduces the efficiency. The equalizer presented in [38] uses one transformer as an energy carrier. Many high-frequency switches and drivers are used, resulting in complex circuit control.

In [18], an HME structure, which is based on a half-bridge LLC resonant converter and a buck-boost converter, is proposed. It leverages a hierarchical design to enhance the energy flow performance and incorporates a basic C2C topology to facilitate circuit extensibility. However, the double-layer structure necessitates a complex control algorithm. Dual frequency modular multilayer equalizer [39] enables multi-input multioutput balancing operation through multiactive bridge converter and Class-D converter. However, as the number of batteries increases, the design of high-frequency magnetic coupling becomes complicated. In [40], the battery equalizer and

TABLE III
PERFORMANCE COMPARISON OF DIFFERENT EQUALIZERS

Circuit Topology	Type of energy flow	Switching frequency (kHz)	Equalization speed***	Reported efficiency (%)	Multi-cell equalization	Increase of switch voltage stress with # of cells	Autonomous equalization	Pulsating current	Cost** ($)
Buck-boost [12]	C2C	100	Slow	88	Yes	No	Yes	No	7.95
Cuk [13]	C2C	30	Medium	90.1*	No	No	No	No	3.26
LC network [14]	C2C	34.5	Medium	87.9*	No	No	No	Yes	5.77
Flyback/forward [37]	C2C	20	Slow	80.7 & 70.1	No	No	No	Yes	6.69
Transformer carrier [38]	C2C	20	Medium	80.4	No	Yes	No	Yes	2.9
LLC & buck-boost [18]	HME	100 & 200	Fast	86.74 & 89.66*	No	Yes	No	Yes	7.39
Class-D & multi-active-bridge [39]	HME	200 & 13.56k	Fast	74 & 93	No	No	No	Yes	12.06
IRSWVD-SVM [40]	HME	100	Medium	72	Yes	Yes	Yes	No	3.31
LCC converter [21]	S2C	200	Medium	88.1*	No	Yes	No	Yes	3
Stacked buck-boost [22]	S2C	100k	Medium	–	Yes	Yes	Yes	Yes	2.07
AC-Bus SEPIC [23]	S2C	100k	Large	86	No	No	Yes	Yes	2.69
Multiport converter [24]	S2C	100k	Fast	91.1*	Yes	Yes	No	No	13.92
Half-bridge converter [25]	S2C	10k	Medium	88	Yes	Yes	No	Yes	6.42
Parallel-transformers [26]	S2C	150k	Slow	91.7	Yes	Yes	Yes	Yes	2.1
Proposed structure	S2C	200k	Medium	86	Yes	No	Yes	No	2.95

*Power dissipation of the selection switches not mentioned.
**Component cost per unit ($) [41]: MOSFET: $0.34 – $1.75. MOSFET Driver: $1.8. GaN: $2.34. Diode: $0.17 - $0.25. Capacitor: $0.2. Inductor: $0.5. Transformer Core: $0.9. Winding: $0.2. Relay: $0.6 - $2.87.
***Slow: Non-constant current and non-multi-cell equalization; Medium: constant current or multi-cell equalization; Fast: constant current and multi-cell equalization.

supercapacitor charger are combined into a topology, which reduces the number of switches. However, excessive diodes result in significant power losses.

For S2C structures, an LCC resonant converter-based equalizer is proposed in [21]. It realizes constant current equalization with open-loop control. However, the number of required relays is twice the number of the battery cells to perform multiplexing function. Numerous active switches lead to high control complexity and low reliability. In [22], a stacked buck-boost converter that only needs a single switch for the battery string is proposed. However, it is not modularized, as the number of battery cells increases, the voltage stress on the switch also increases. In [23], a multilayer voltage equalizer that provides direct paths between all the modules of the battery pack is proposed. Nevertheless, multiwinding transformer are commonly used in MC. In addition, when the number of batteries changes, it is necessary to redesign the transformer to increase the number of windings. In [24], an MC-based equalizer is proposed. It achieves simultaneous equalization of multiple cells. However, plenty of MOSFETs lead to low reliability and high cost. The authors in [24], [25], and [26] proposed structures using multiwinding transformers, where their implementation in large-scale systems is a challenge.

All structures, except [26], can perform equalization without the need for an external power source. However, most structures lack the flexibility to scale the system for varying numbers of battery cells within a string. Only references [18], [23], and [39], and the proposed method are modular based, allowing for adaptable scaling in large-scale battery storage systems. Among these, the proposed method requires the fewest switching devices and no selection switches. Regarding passive components, the proposed method necessitates more components for filtering purposes to maintain a relatively constant charging or discharging current across the battery cells, contrasting with other methods that exhibit pulsating currents.

Table III provides a performance evaluation covering various aspects including the type of energy flow as outlined in Section I, switching frequency, balancing speed, power efficiency, capability of multicell equalization, impact of increasing the number of battery cells on the voltage stress of switching devices, autonomous equalization functionality, and simple cost analysis. Except for [41] that operates at 13.6 MHz, the equalizers generally operate at lower frequencies ranging between 10 and 200 kHz. Reported efficiency levels fall within the range of 70.1%–93%, with the proposed method achieving an efficiency of 86%. As discussed in Section III, the conduction loss of the diodes is the main source of power dissipation. Choosing components with small parasitic parameters can enhance equalization efficiency and performance.

Among the compared methods, only [12], [22], [24], [25], [26], and [40], and the proposed approach support multicell equalization that all battery cells undergo charging or discharging simultaneously. In addition, only [12], [13], [14], [23], [37], and [39], and the proposed method demonstrate voltage stress on the switching devices independent of the number of cells, while only [12], [22], [23], [26], and [40] and the proposed method offer autonomous equalization functionality that battery cells will be charged or discharged independently as needed. The analysis also briefly addresses the overall cost of components

used in the equalizers, with component values based on prices listed in [41].

Based on Tables II and III, it can be noted that the proposed method excels among modular-based systems. It can autonomously balance multiple cells, maintains consistent voltage stress on the switching device regardless of the battery cell count, and importantly, supports a steady charging and discharging current that can improve the longevity of the battery cells.

The equalization speed is influenced by the equalization current, which is affected by several factors, such as the duty cycle of the main switch. Among various configurations, the C2C structure offers a higher equalization speed due to its more direct charge transfer. However, different structures have different numbers of batteries that can be balanced simultaneously. Moreover, in applications where the equalization process operates continuously, the speed of equalization becomes noncritical.

VII. Conclusion

An ABEM, which employs an energy circulation technique to equalize the voltage across individual battery cells in a series-connected batteries, is presented. No selection switches and multiwinding transformers are required. The module, designed based on the ZETA-derived converter structure, features two power conversion stages. The first one converts the battery string voltage into a high-frequency ac voltage to form a capacitively coupled ac link. The second stage contains multiple diode-based rectifiers with their inputs connected to the ac link via coupling capacitors and their outputs connected in series to individual battery cells. The architecture not only balances the battery cell voltages within a module but also enables the connection of multiple modules via the ac link. This allows individual battery cells to be charged from or discharged to other cells within the same module or across different modules. This stands out among S2C systems for its ability to balance multiple cells independently, maintain consistent voltage stress on switching devices regardless of the number of battery cells, and support a charging and discharging current with small ripple that can enhance battery longevity. The system is adaptable for strings with varying number of battery cells, making it suitable for use in large-scale battery setups. Two four-cell modules have been constructed and evaluated successfully for the equalization of eight 3.6 V, 18 650 batteries.

Appendix

Based on (37), the resonant frequency of the circuit can be obtained by solving ω for $|Z_e| = 0$. The RHS of (37) gives

$$\omega^2 = \frac{-b + \sqrt{b^2 - 4ac}}{2a} \tag{42}$$

where

$$\begin{aligned} a &= n^2 C_{\text{oss}} L_m L_g L_e C_e C_A C_B \\ &\quad + n^2 C_{\text{oss}} (L_g L_e C_e C_A C_B + L_e L_m C_e C_A C_B) \\ b &= -[n^2 C_{\text{oss}} L_g (C_A C_B + C_A C_e + C_B C_e) \\ &\quad + L_m C_e C_A C_B + n^2 L_e C_e C_A C_B \\ &\quad + n^2 C_{\text{oss}} L_m (C_A C_B + C_A C_e + C_B C_e)] \\ c &= n^2 (C_A C_B + C_A C_e + C_B C_e). \end{aligned} \tag{43}$$

Thus, T_{ds} can be expressed as

$$T_{ds} = \frac{2\pi}{\omega} = \frac{2\pi\sqrt{2a}}{\sqrt{-b + \sqrt{b^2 - 4ac}}}. \tag{44}$$

References

[1] N. Hasanpour and S. A. Khajehoddin, "Energy conservation versus charge conservation law for modeling and analyzing cell equalizers," *IEEE Trans. Power Electron.*, vol. 38, no. 11, pp. 14638–14651, Nov. 2023.

[2] M. A. Hannan et al., "SOC estimation of Li-ion batteries with learning rate-optimized deep fully convolutional network," *IEEE Trans. Power Electron.*, vol. 36, no. 7, pp. 7349–7353, Jul. 2021.

[3] J. Yang, Y. Cai, and C. C. Mi, "State-of-health estimation for lithium-ion batteries based on decoupled dynamic characteristic of constant-voltage charging current," *IEEE Trans. Transp. Electrific.*, vol. 8, no. 2, pp. 2070–2079, Jun. 2022.

[4] G. Liang et al., "A constrained intersubmodule state-of-charge balancing method for battery energy storage systems based on the cascaded H-bridge converter," *IEEE Trans. Power Electron.*, vol. 37, no. 10, pp. 12669–12678, Oct. 2022.

[5] H. Yin, Y. Li, Y. Kang, and C. Zhang, "A two-stage sorting method combining static and dynamic characteristics for retired lithium-ion battery echelon utilization," *J. Energy Storage*, vol. 64, Aug. 2023, Art. no. 107178.

[6] T. A. Fagundes et al., "A modified redundancy-based energy management system for microgrids: An SoC enhancement approach," *IEEE Trans. Ind. Electron.*, vol. 71, no. 10, pp. 12379–12388, Oct. 2024.

[7] H. Zhang, X. Hu, Z. Hu, and S. J. Moura, "Sustainable plug-in electric vehicle integration into power systems," *Nat. Rev. Electr. Eng.*, vol. 1, no. 1, pp. 35–52, Jan. 2024.

[8] H. Lin, H. S.-H. Chung, R. Shen, and Y. Xiang, "Enhancing stability of DC cascaded systems with CPLs using MPC combined with NI and accounting for parameter uncertainties," *IEEE Trans. Power Electron.*, vol. 39, no. 5, pp. 5225–5238, May 2024.

[9] N. Yang, H. Hofmann, J. Sun, and Z. Song, "Remaining useful life prediction of lithium-ion batteries with limited degradation history using random forest," *IEEE Trans. Transp. Electrific.*, vol. 10, no. 3, pp. 5049–5060, Sep. 2024.

[10] G. Noh, J. Lee, and J.-I. Ha, "Design and analysis of single-inductor power converter for both battery balancing and voltage regulation," *IEEE Trans. Ind. Electron.*, vol. 69, no. 3, pp. 2874–2884, Mar. 2022.

[11] Y. Izadi and R. Beiranvand, "A comprehensive review of battery and supercapacitor cells voltage-equalizer circuits," *IEEE Trans. Power Electron.*, vol. 38, no. 12, pp. 15671–15692, Dec. 2023.

[12] T. H. Phung, A. Collet, and J.-C. Crebier, "An optimized topology for next-to-next balancing of series-connected lithium-ion cells," *IEEE Trans. Power Electron.*, vol. 29, no. 9, pp. 4603–4613, Sep. 2014.

[13] S. K. Dam and V. John, "Low-frequency selection switch based cell-to-cell battery voltage equalizer with reduced switch count," *IEEE Trans. Ind. Applicat.*, vol. 57, no. 4, pp. 3842–3851, Jul./Aug. 2021.

[14] C. Zhang, N. Cui, Z. Zhou, Y. Shang, B. Duan, and Q. Zhang, "Multi-cell-to-Multi-Cell equalizers based on matrix and half-bridge LC converters for series-connected battery strings," *IEEE J. Emerg. Sel. Topics Power Electron.*, vol. 8, no. 2, pp. 1755–1766, Jun. 2020.

[15] M. Evzelman, M. M. Ur Rehman, K. Hathaway, R. Zane, D. Costinett, and D. Maksimovic, "Active balancing system for electric vehicles with incorporated low-voltage bus," *IEEE Trans. Power Electron.*, vol. 31, no. 11, pp. 7887–7895, Nov. 2016.

[16] S. K. Dam and V. John, "A modular fast cell-to-cell battery voltage equalizer," *IEEE Trans. Power Electron.*, vol. 35, no. 9, pp. 9443–9461, Sep. 2020.

[17] K. Eguchi, A. Shibata, W. Do, and F. Asadi, "Design and analysis of an inductor-less cross-coupled voltage equalizer," *Energy Rep.*, vol. 6, pp. 1151–1156, Dec. 2020.

[18] F. Peng, H. Wang, and Z. Wei, "An *LLC*-Based highly efficient S2M and C2C hybrid hierarchical battery equalizer," *IEEE Trans. Power Electron.*, vol. 35, no. 6, pp. 5928–5937, Jun. 2020.

[19] M. Uno and K. Yoshino, "Modular equalization system using dual phase-shift-controlled capacitively-isolated dual active bridge converters to equalize cells and modules in series-connected lithium-ion batteries," *IEEE Trans. Power Electron.*, vol. 36, no. 3, pp. 2983–2995, Mar. 2021.
[20] J. Nie, R. Fu, C. Cai, J. Ma, Z. Shu, and L. Ma, "A high efficiency battery equalizing circuit based on half bridge topology with multiport transformer," *IEEE Trans. Ind. Electron.*, vol. 71, no. 3, pp. 2522–2532, Mar. 2024.
[21] Z. Wei, F. Peng, and H. Wang, "An LCC based string-to-cell battery equalizer with simplified constant current control," *IEEE Trans Power Electron.*, vol. 37, no. 2, pp. 1816–1827, Feb. 2022.
[22] M. Uno and K. Tanaka, "Single-switch cell voltage equalizer using multistacked buck-boost converters operating in discontinuous conduction mode for series-connected energy storage cells," *IEEE Trans. Veh. Technol.*, vol. 60, no. 8, pp. 3635–3645, Oct. 2011.
[23] N. Hasanpour, M. R. Mohammadi, A. Tavakoli, and S. A. Khajehoddin, "Modular voltage equalizer circuit with AC-bus inter-modules connection," *IEEE Trans. Transp. Electrific.*, vol. 10, no. 1, pp. 682–698, Mar. 2024.
[24] X. Qi, Y. Wang, M. Fang, H. Wang, Y. Wang, and Z. Chen, "A family of integrated cascade multiport converters for centralized equalization systems: Derivation, analysis, and verification," *IEEE Trans. Power Electron.*, vol. 38, no. 6, pp. 7398–7415, Jun. 2023.
[25] Y. Shang, S. Zhao, Y. Fu, B. Han, P. Hu, and C. Mi, "A lithium-ion battery balancing circuit based on synchronous rectification," *IEEE Trans. Power Electron.*, vol. 35, no. 2, pp. 1637–1648, Feb. 2020.
[26] L. Liu, Z. Yan, B. Xu, P. Zhang, C. Cai, and H. Yang, "A highly scalable integrated voltage equalizer based on parallel-transformers for high-voltage energy storage systems," *IEEE Trans. Ind. Electron.*, vol. 71, no. 1, pp. 595–603, Jan. 2024.
[27] J. Carter, Z. Fan, and J. Cao, "Cell equalisation circuits: A review," *J. Power Sources*, vol. 448, pp. 227–489, Feb. 2020.
[28] W. Liao, Y. Chen, J. Zeng, Z. Lai, and J. Liu, "Topology, analysis, and modeling of voltage equalizers based on reutilization technique for supercapacitor storage system," *IEEE Trans. Transp. Electrific.*, vol. 7, no. 4, pp. 2293–2305, Dec. 2021.
[29] M. M. Hoque, M. A. Hannan, A. Mohamed, and A. Ayob, "Battery charge equalization controller in electric vehicle applications: A review," *Renew. Sustain. Energy Rev.*, vol. 75, pp. 1363–1385, Aug. 2017.
[30] Z. Wei, H. Wang, Y. Lu, D. Shu, G. Ning, and M. Fu, "Bidirectional constant current string-to-cell battery equalizer based on L2C3 resonant topology," *IEEE Trans. Power Electron.*, vol. 38, no. 1, pp. 666–677, Jan. 2023.
[31] Z. Zhang, H. Gui, D. J. Gu, Y. Yang, and X. Ren, "A hierarchical active balancing architecture for lithium-ion batteries," *IEEE Trans. Power Electron.*, vol. 32, no. 4, pp. 2757–2768, Apr. 2017.
[32] F. Qu, Q. Luo, H. Liang, D. Mou, P. Sun, and X. Du, "Systematic overview of active battery equalization structures: Mathematical modeling and performance evaluation," *IEEE Trans. Energy Conver.*, vol. 37, no. 3, pp. 1685–1703, Sep. 2022.
[33] R. Zhang, S. Wang, Z. Cao, and H. S.-H. Chung, "A galvanic-isolated automatic equalization charging system for series-connected cells or battery strings," *IEEE Trans. Ind. Electron.*, vol. 71, no. 11, pp. 13943–13954, Nov. 2024.
[34] G. Zhao, C. Zhang, B. Duan, Y. Shang, Y. Kang, and R. Zhu, "State-of-health estimation with anomalous aging indicator detection of lithium-ion batteries using regression generative adversarial network," *IEEE Trans. Ind. Electron.*, vol. 70, no. 3, pp. 2685–2695, Mar. 2023.
[35] H. Wang, M. Rasheed, R. Hassan, M. Kamel, S. Tong, and R. Zane, "Life-extended active battery control for energy storage using electric vehicle retired batteries," *IEEE Trans. Power Electron.*, vol. 38, no. 6, pp. 6801–6805, Jun. 2023.
[36] R. C. Viero and F. S. dos Reis, "Dynamic modeling of a ZETA converter in DCM applied to low power renewable sources," in *Proc. 2011 IEEE Energy Convers. Congr. Expo.*, Sep. 2011, 685–691.
[37] Y. Chen, X. Liu, Y. Cui, J. Zou, and S. Yang, "A MultiWinding transformer cell-to-cell active equalization method for lithium-ion batteries with reduced number of driving circuits," *IEEE Trans. Power Electron.*, vol. 31, no. 7, pp. 4916–4929, Jul. 2016.
[38] K. M. Lee, S. W. Lee, Y. G. Choi, and B. Kang, "Active balancing of li-ion battery cells using transformer as energy carrier," *IEEE Trans. Ind. Electron.*, vol. 64, no. 2, pp. 1251–1257, Feb. 2017.
[39] M. Liu, Y. Chen, Y. Elasser, and M. Chen, "Dual frequency hierarchical modular multilayer battery balancer architecture," *IEEE Trans. Power Electron.*, vol. 36, no. 3, pp. 3099–3110, Mar. 2021.
[40] X. Tan, Y. Chen, J. Zeng, W. Liao, and J. Liu, "An integrated self-modularized battery equalizer and supercapacitor charger for hybrid electric vehicle energy storage system," *IEEE Trans. Veh. Technol.*, vol. 73, no. 7, pp. 9865–9877, Jul. 2024.
[41] "Digikey electronics electronic components distributor," Jul. 2024. [Online]. Available: https://www.digikey.com

Zhengqi Wei (Graduate Student Member, IEEE) received the B.S. degree in electronic information science and technology from Shaanxi Normal University, Xi'an, China, in 2019, and the M.S. degree in electronic science and technology from ShanghaiTech University, Shanghai, China, in 2022. He is currently working toward the Ph.D. degree in electrical engineering with the City University of Hong Kong, Hong Kong.

His research interests include power electronics, battery management system, and battery equalization.

Henry Shu-Hung Chung (Fellow, IEEE) received the B.Eng. and Ph.D. degrees in electrical engineering from Hong Kong Polytechnic University, Hong Kong, in 1991 and 1994, respectively.

Since 1995, he has been with the City University of Hong Kong, Hong Kong, where he is currently the Dean of Students, a Chair Professor with the Department of Electrical Engineering, and the Director with the Centre for Smart Energy Conversion and Utilization Research. He has edited two books, authored eight research book chapters, and more than 500 technical papers including 240 refereed journal papers in his research areas, and holds 80 patents. His research interests include renewable energy conversion technologies, lighting technologies, energy harvesting, smart grid technologies, and computational intelligence for power electronic systems.

Dr. Chung was the recipient of 2021 IEEE Power Electronics Society R. David Middlebrook Achievement Award, CityU Outstanding Research Award in 2020, and CityU Teaching Excellence Awards in 2018 and 2022, respectively. He is currently an Associate Editor for IEEE TRANSACTIONS ON POWER ELECTRONICSand IEEE JOURNAL OF EMERGING AND SELECTED TOPICS IN POWER ELECTRONICS. He was the Editor-in-Chief for the IEEE POWER ELECTRONICS LETTERS 2014–2018. He was also the Chair of the Technical Committee of the High-Performance and Emerging Technologies, IEEE Power Electronics Society in 2010–2014. He was the recipient of numerous industrial awards for his invented energy saving technologies.

Ruihong Zhang (Member, IEEE) received the B.Eng. degree in computer science and the M.Eng. degree in electrical engineering from the Harbin Institute of Technology, Shenzhen, China, in 2005 and 2008, respectively, and the Ph.D. degree in electrical engineering from the City University of Hong Kong, Hong Kong, in 2013.

From 2014 to 2015, she was a Postdoctoral Fellow with the City University of Hong Kong. From 2016 to 2018, she was an Associate Professor with Northwestern Polytechnical University, Xi'an, China, and from 2018 to 2024, with the Harbin Institute of Technology, Shenzhen, China. Since 2024, she has been a Chief Engineer with BYD Company Ltd., Shenzhen, China. Her research interests include the lighting systems, wireless power transfer, power-factor correction, resonant converters, as well as ac/dc and dc/dc converters.